

EVIDENCE FOR A ~ 300 MEGAPARSEC SCALE UNDER-DENSITY IN THE LOCAL GALAXY DISTRIBUTION

R. C. KEENAN¹, A. J. BARGER^{2,3,4}, L. L. COWIE⁴

Draft version December 2, 2024

ABSTRACT

Galaxy counts and recent measurements of the luminosity density in the near-infrared (NIR) have indicated the possibility that the local universe may be under-dense on scales of several hundred megaparsecs. The presence of a large-scale under-density in the local universe could introduce significant biases into the interpretation of cosmological observables, and, in particular, into the inferred effects of dark energy on the expansion rate. Here we measure the K -band luminosity density as a function of redshift to test for such a local under-density. We select galaxies from the UKIRT Infrared Deep Sky Large Area Survey (UKIDSS-LAS) and use spectroscopy from the Sloan Digital Sky Survey (SDSS) and other redshift surveys to generate a K -selected catalog of $\sim 35,000$ galaxies that is $> 90\%$ spectroscopically complete to $K_{AB} = 16.3$. The relative depth and wide area of our sample allow for a detailed measurement of the K -band luminosity density as a function of redshift in the range $0.005 < z < 0.2$. We find that the overall shape of the $z = 0$ rest-frame K -band luminosity function ($M^* = -21.38 \pm 0.04$ and $\alpha = -1.02 \pm 0.03$) appears to be relatively constant as a function of environment and redshift out to $z \sim 0.2$. We find a local ($z < 0.07$) luminosity density that is in good agreement with previous studies. At $z > 0.07$ we detect a rising luminosity density, and at $z > 0.1$, it is roughly ~ 1.5 times higher than that measured locally. This suggests that the stellar mass density as a function of redshift follows a similar trend. Assuming that luminous matter traces the underlying dark matter distribution, this implies that the local mass density of the universe may be lower than the global value on a scale and amplitude sufficient to introduce significant biases into the determination of basic cosmological observables, such as the expansion rate. An under-density of roughly this scale and amplitude would be sufficient to resolve the apparent tension between direct measurements of the Hubble constant and those inferred by Planck.

Subject headings: cosmology: observations — galaxies: fundamental parameters

1. INTRODUCTION

The universe is generally assumed to be isotropic and homogeneous on very large scales. This allows for the development of cosmological models and observations to constrain those models, provided that the observations are made over a sufficiently large volume to average over so called “cosmic variance”, or systematic measurement biases due to large-scale structure. Observations of the cosmic microwave background (CMB) indicate the universe was very homogeneous at $z \sim 1100$ and measurements of the kinematic Sunyaev-Zeldovich (kSZ) effect appear to indicate that the present day universe is homogeneous on scales greater than ~ 1 Gpc (García-Bellido & Haugbølle 2008; Zhang & Stebbins 2011). However, the large-scale homogeneity of the universe on smaller scales has not been measured directly.

Observed large-scale structures, such as the > 400 Mpc Sloan Great Wall (Gott et al. 2005), demonstrate the existence of inhomogeneity on very large scales. In addition, it has been shown that voids on similarly large scales may explain the “cold spots” in the CMB

(Inoue & Silk 2006). While such structures had previously been thought to be departures from the expectation of Λ CDM cosmology (Sheth & Diaferio 2011), it has now been found that such large-scale structures are not only to be expected in the current concordance cosmology, but also that even larger structures are likely to be discovered as survey volumes increase (Park et al. 2012).

Recent cosmological modeling efforts have demonstrated that large-scale structure in the local universe may introduce significant systematic errors into the measurement of cosmological observables and hence the interpretation of these observables in the context of a given cosmological model (for recent reviews see Bolejko et al. 2011; Clarkson 2012). In particular, so called “void models” place the observer inside a large local under-density to provide for the apparent acceleration of the expansion of the universe (Moffat & Tatarski 1992, 1995; Célérier 2000; Tomita 2000, 2001a,b; Iguchi et al. 2002; Alnes et al. 2006; Chung & Romano 2006; Enqvist & Mattsson 2007; Yoo et al. 2008; Garcia-Bellido & Haugbølle 2008; Alexander et al. 2009; García-Bellido & Haugbølle 2009; February et al. 2010; Célérier et al. 2010; Biswas et al. 2010; Marra & Pääkkönen 2010; Clarkson & Maartens 2010; Bolejko & Sussman 2011; Nishikawa et al. 2012; Valkenburg 2012).

The basic idea underlying these void models is that if an observer lives near the center of a large under-density, then that observer will witness a local expansion of the

¹ Academia Sinica Institute of Astronomy and Astrophysics, P.O. Box 23-141, Taipei 10617, Taiwan

² Department of Astronomy, University of Wisconsin-Madison, 475 North Charter Street, Madison, WI 53706, USA

³ Department of Physics and Astronomy, University of Hawaii, 2505 Correa Road, Honolulu, HI 96822, USA

⁴ Institute for Astronomy, University of Hawaii, 2680 Woodlawn Drive, Honolulu, HI 96822, USA

universe that is faster than the global expansion. This would result in a locally measured Hubble constant that is larger than the global expansion rate and appear observationally as an accelerating expansion.

In their current form, void models without a cosmological constant do not appear to be viable alternatives to dark-energy-dominated universes, as they have problems in simultaneously fitting all cosmological observables (García-Bellido & Haugbølle 2008; Zibin et al. 2008; Moss et al. 2011; Zhang & Stebbins 2011; Riess et al. 2011; Zumalacárregui et al. 2012). However, the exploration of these types of cosmological models—and other models which explore the effects of large-scale inhomogeneity—has highlighted the need for a more thorough understanding of extremely large-scale structure in the local universe (Marra & Notari 2011; Marra et al. 2012, 2013; Bull & Clifton 2012; Mishra et al. 2012, 2013; Valkenburg et al. 2012, 2013).

In particular, “minimal void” scenarios (e.g., Alexander et al. 2009; Bolejko & Sussman 2011) have shown that very simple models placing the observer near the center of an under-density that is $\sim 250 h^{-1}$ Mpc in radius (extending to $z \sim 0.08$) and roughly half the density of its surroundings are sufficient to explain the acceleration observed via type Ia supernovae. While these models are simplistic, they make clear that an observer’s location with respect to large-scale structures could have profound implications for that observer’s measurement of cosmological observables.

In this study, we wish to make an estimate of the mass density of the nearby universe as a function of redshift to test for large-scale inhomogeneity, and in particular, for a large local under-density. While we cannot directly probe the underlying dark matter distribution, we can make a robust estimate of the near-infrared (NIR) luminosity density, which is a good tracer of the overall stellar mass density (e.g., de Jong 1996; Bell & de Jong 2001; Bell et al. 2003; Kirby et al. 2008). The stellar masses of galaxies, on average, have been shown to be correlated with the mass of their host dark matter halos (e.g., Wang et al. 2012). Furthermore, simulations have shown that on much larger (~ 100 Mpc) scales at low redshift, the spatial distribution of baryons should be an unbiased tracer of the underlying dark matter distribution (Angulo et al. 2013).

Thus, in terms of the linear bias parameter, here we will assume $b = 1$ in the relation $\delta_g = b\delta$, where δ_g is the relative density contrast given by the distribution of galaxies, i.e., $(\rho_{\text{stars},z} - \bar{\rho}_{\text{stars}})/\bar{\rho}_{\text{stars}}$, and δ is the total mass density contrast, $(\rho_z - \bar{\rho})/\bar{\rho}$. At optical wavelengths, the linear bias parameter has been observed to approach unity at low redshifts (e.g., Marinoni et al. 2005), and in the NIR, Maller et al. (2005) have measured a value in the K -band of $b_K(z \approx 0) = 1.1 \pm 0.2$, suggesting the NIR bias parameter follows a similar trend.

Therefore, a measurement of the NIR luminosity density can provide an estimate of the underlying mass density of the universe. Likewise, a measured change in NIR luminosity density as a function of redshift could signal a corresponding change in the underlying total mass density. Thus, in the NIR at low redshifts, where dust extinction is minimal and K -corrections are small and nearly independent of galaxy type, statistical studies of galaxies provide a means of probing local large-scale

structure.

Several studies of NIR galaxy counts have found that the local space density of galaxies appears to be low by $\sim 25 - 50\%$ compared to the density at distances of $\sim 300 h^{-1}$ Mpc or beyond $z \sim 0.1$ (Huang et al. 1997; Frith et al. 2003, 2005; Busswell et al. 2004; Keenan et al. 2010a). If the space density of galaxies is rising as a function of redshift, then a corresponding rise in NIR luminosity density should also be present.

In Keenan et al. (2012), we probed the NIR luminosity function (LF) just beyond the local volume at redshifts of $z \sim 0.2$. We found that the NIR luminosity density at $z \sim 0.2$ appears to be $\sim 30\%$ higher than that measured at $z \sim 0.05$. This measured excess could be considered a conservative underestimate, because we avoided known over-densities, such as galaxy clusters, in our study. We note that our result cannot be considered conclusive, given possible systematics due to cosmic variance in our measurement. However, taken in the context of other measurements of the NIR luminosity density from the literature, our result is consistent with other studies that found a higher luminosity density at $z > 0.1$ than that found locally. Furthermore, we showed that all measurements of the luminosity density could be considered roughly consistent with the void radial density profile from Bolejko & Sussman (2011), which they claim could mimic the apparent acceleration of the expansion of the universe.

In the past, wide-area NIR surveys have generally not gone deep enough to probe beyond the very local universe, and deep surveys have been carried out over relatively small solid angles, such that good counting statistics cannot be achieved at lower redshifts. The result is that, in a study such as that performed in Keenan et al. (2012), we are comparing measurements made with quite different photometry and methodology, and the results may suffer from unknown biases.

Recently, however, the completion of the relatively deep and wide UKIRT Infrared Deep Sky Large Area Survey (UKIDSS-LAS, Lawrence et al. 2007), combined with spectroscopy from the Sloan Digital Sky Survey (SDSS, York et al. 2000), the Two-degree Field Galaxy Redshift Survey (2dFGRS, Colless et al. 2001), and other spectroscopic data from the archives, provides for a NIR-selected spectroscopic sample of galaxies that is both wide enough on the sky and deep enough photometrically to sample a relatively broad range in redshifts in the nearby universe with good statistics. In this paper, we draw a K -band selection of galaxies from the UKIDSS-LAS that is highly spectroscopically complete. We then study the K -band galaxy LF over a large volume in the redshift range $0.005 < z < 0.2$. With these data we are able, for the first time, to measure the K -band galaxy LF as a function of redshift using consistent photometry and methodology.

The structure of this paper is the following. We discuss the sample selection in Section 2. We estimate the K -band luminosity density as a function of redshift and possible biases in our measurements in Section 3. We summarize our results in Section 4. Unless otherwise noted, all magnitudes listed here are in the AB magnitude system ($m_{\text{AB}} = 23.9 - 2.5 \log_{10} f_{\nu}$ with f_{ν} in units of μJy). We assume $\Omega_M = 0.3$, $\Omega_{\Lambda} = 0.7$, and $h = 0.7$ in our calculations.

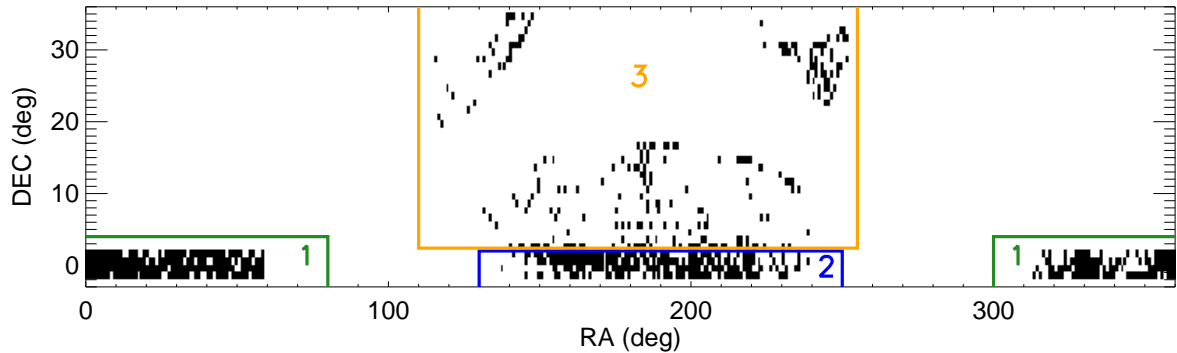


Figure 1. The region on the sky where the UKIDSS-LAS DR8 and the SDSS DR9 overlap and the spectroscopic completeness is $> 90\%$ ($\sim 536.9 \text{ deg}^2$ total). The black rectangles represent $1^\circ \times 1^\circ$ areas of high completeness within the overlap region. The boxes drawn in green, blue, and orange denote the three subregions in this sample that are subsequently dealt with separately to address possible biases and cosmic variance in this study.

2. CATALOG GENERATION

To create a stellar mass selected sample, we have retrieved data from the WFCam Science Archive (WSA) for all galaxies with NIR photometry in the UKIDSS-LAS DR8 in the K -band ($K_{\text{Vega}} < 14.4$, which is equivalent to $K_{\text{AB}} < 16.3$), where overlap with the SDSS, the 2dFGRS, and other surveys provides for highly complete spectroscopy of bright galaxies ($> 90\%$ complete for $K_{\text{AB}} = 16.3$). This region of sky covers 536.9 deg^2 , and the selection contains 35,342 galaxies at a median redshift of $z \sim 0.1$.

We then used the SDSS-III Sky Server CasJobs⁵ interface to retrieve optical photometry and redshifts from the SDSS DR9 over the areas covered in all bands (Y, J, H , and K) in the UKIDSS-LAS. We then cross-correlated the positions of the K -selected objects with those from the SDSS using a search radius of $2''$.

A small fraction ($< 1\%$) of objects identified in the UKIDSS catalogs did not have a counterpart within $< 2''$ in the SDSS. We found that these objects generally appeared to be spurious K -band detections (checking by eye in the imaging data from UKIDSS), so we excluded these objects from the final catalog. Thus, all of the UKIDSS K -band selected objects in our catalog have counterparts classified as primary target galaxies in the SDSS. We find that 95% of UKIDSS objects matched to SDSS counterparts have angular separations of $< 0''.5$, and the average separation between UKIDSS objects and their SDSS counterparts is $0''.2$.

We also downloaded the 2dFGRS redshift catalogs from the VizieR online service⁶. We cross-matched 2dF objects to their UKIDSS counterparts within a radius of $2''$. Cross-correlation with the 2dFGRS significantly improved overall completeness in the 2dF equatorial region from $10^h < \text{RA} < 15^h$ (subregion 2 denoted in Figure 1). We also cross-correlated with published redshifts in the NASA-Sloan Atlas⁷ and the NASA/IPAC Extragalactic Database⁸ to augment the completeness of the sample.

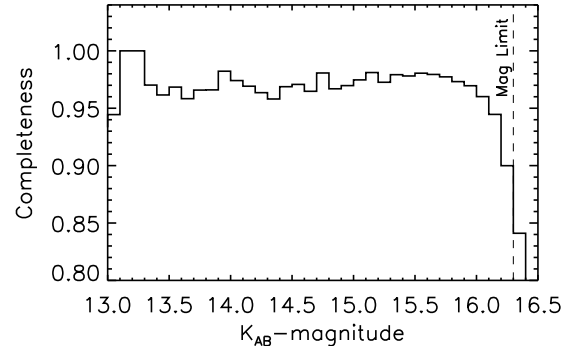


Figure 2. Completeness as a function of K -band apparent magnitude. The average completeness of the full sample of 35,342 galaxies with $K_{\text{AB}} < 16.3$ is $\sim 95\%$.

We restricted our final catalog to regions on the sky which are $> 90\%$ spectroscopically complete at $K_{\text{AB}} < 16.3$ in order to minimize possible biases associated with the fact that our sample is selected in the K -band, while the targets for the surveys providing the redshifts for this work were primarily optically selected. This resulted in a catalog of 35,342 galaxies over the 536.9 deg^2 region shown in Figure 1, after excluding stars from the catalog, as we describe in the following subsection. We show the completeness of the sample as a function of apparent magnitude in Figure 2 and the redshift distribution in Figure 3.

2.1. Star-Galaxy Separation

We investigated the $g-J$ vs. $J-K$ color-color diagram for objects in our catalog to determine the reliability of the star-galaxy classifiers offered in the WSA and SDSS archives (UKIDSS “mergedclass” and SDSS “type”). We show a gJK color-color diagram for $3''$ aperture magnitude colors in Figure 4. Orange points show objects classified by morphology as extended in both UKIDSS and the SDSS (UKIDSS $\text{mergedclass} = -1$ and SDSS $\text{type} = 6$). Light blue points show objects classified as point sources in both UKIDSS and the SDSS (UKIDSS $\text{mergedclass} = 1$ and SDSS $\text{type} = 3$). Red points show

⁵ skyserver.sdss3.org/CasJobs

⁶ <http://vizier.cfa.harvard.edu/viz-bin/VizieR-3>

⁷ www.nsatalas.org

⁸ ned.ipac.caltech.edu

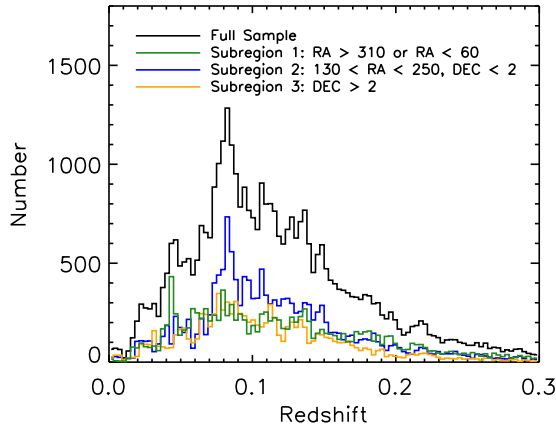


Figure 3. The redshift histogram for the spectroscopic sample of galaxies in this study. Subregion 2 overlaps with the Sloan Great Wall identified by Gott et al. (2005), and the peak in the redshift histogram in this region near $z \sim 0.08$ is primarily due to this structure.

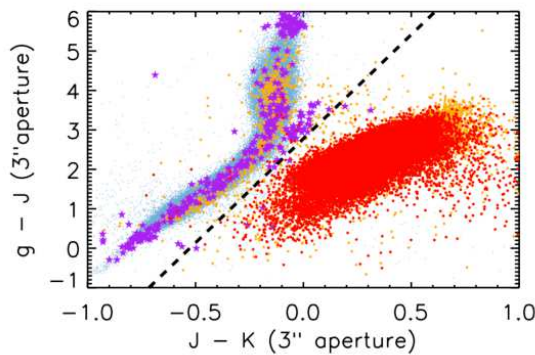


Figure 4. A $3''$ aperture magnitude color-color separation for all objects at $K < 16.3$ in the raw sample drawn from the WSA and SDSS Skyserver. Orange points show objects classified by morphology as extended in both UKIDSS and the SDSS (UKIDSS *mergedclass* = -1 and SDSS *type* = 6). Light blue points show objects classified as point sources in both UKIDSS and the SDSS (UKIDSS *mergedclass* = 1 and SDSS *type* = 3). Red points show spectroscopically identified galaxies. Purple stars show spectroscopically identified stars. The dashed line shows the best color separation boundary between stars and galaxies: $g - J = 5.28 \times [J - K] + 2.78$. Approximately $\sim 2\%$ of extended sources lie above the separation boundary and $\sim 0.5\%$ of point sources lie below. Based on analyses described in Section 2.1, we conclude that by excluding all sources above the separation boundary, as well as all sources identified by morphology as point sources in the SDSS and WSA (regardless of color), we can achieve a star-galaxy separation that is robust at better than the 1% level.

spectroscopically identified galaxies. Purple stars show spectroscopically identified stars. The dashed line shows the best color separation boundary between stars and galaxies: $g - J = 5.28 \times [J - K] + 2.78$. Approximately $\sim 2\%$ of extended sources lie above the separation boundary and $\sim 0.5\%$ of point sources lie below.

Next, we looked at the images in the SDSS Sky Server database of the point sources that lie below the separation boundary and the extended sources that lie above. For these point sources, it was clear from the SDSS imag-

ing that they are point-like in morphology. We expect that most of these objects are stars with rare colors or bad photometry in one band (with the exception of a few quasars, which are not of interest for this study).

The vast majority of the objects classified as extended that lie above the separation boundary lie along the stellar main sequence for this color separation. Upon investigating the imaging for these sources, we found that, while there are definitely a few galaxies among them, the vast majority ($\sim 99\%$) look like point sources that are either smeared out a bit or blended with another object. Thus, we conclude that the majority of objects that are classified as extended but lie above the boundary are, in fact, stars.

We note that 15 spectroscopically confirmed galaxies lie above the separation boundary. Upon closer inspection of SDSS imaging for these sources, we found that roughly a third appeared to be point-sources on the stellar main sequence (likely stars misclassified as galaxies due to noisy spectra). Another third appeared to be galaxies blended with a star, and the final third appeared to be galaxies by morphology, but with stellar colors. There are only a handful of spectroscopically confirmed stars that lie below the separation boundary, and all appear to be point sources.

Based on these analyses, we conclude that by excluding all sources above the separation boundary described in Figure 4, as well as all sources identified by morphology as point sources in the SDSS and WSA (regardless of color), we can achieve a star-galaxy separation that is robust at better than the 1% level.

2.2. Petrosian Aperture Clipping in UKIDSS Photometry

The sky subtraction algorithm in the pipeline for UKIDSS photometry is such that there exists an upper limit of $6''$ on the Petrosian aperture radius (corresponding to a circular aperture with a radius of $12''$). This causes the total flux from galaxies that subtend large solid angles to be underestimated. This implies that if we use Petrosian magnitudes, then for some galaxies we will underestimate their luminosities, while other galaxies will be lost entirely from the sample, because the aperture clipping has pushed them to a fainter apparent magnitude than the selection limit of the sample.

We retrieved the K -band Petrosian aperture radii for our sample from the WSA and found that roughly $\sim 10\%$ of galaxies in the sample had their Petrosian apertures clipped at $6''$. We show the fraction of galaxies for which the Petrosian aperture was clipped at $6''$ as a function of redshift in Figure 5. Clearly, the underestimation of total flux is a much stronger effect at low redshift ($z < 0.1$). Thus, in general, brighter (larger) galaxies at low redshift are most strongly affected by Petrosian aperture clipping.

Instead of omitting galaxies for which the Petrosian apertures were clipped (e.g., Smith et al. 2009), we have devised a method to compensate for the effects of the underestimation of flux. Short of redoing all the photometry, there is no way to know exactly what fraction of light was lost due to the aperture clipping. However, for each galaxy the WSA provides photometry for circular apertures ranging in size from $1''$ to $12''$ in radius. Using these measurements, we determined a rough light curve for each galaxy affected by Petrosian aperture clipping.

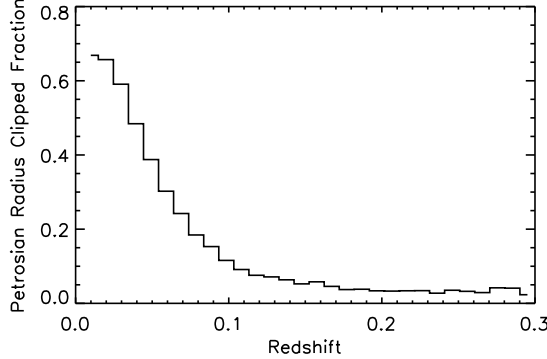


Figure 5. The fraction of galaxies with their Petrosian aperture clipped at $6''$ as a function of redshift in the UKIDSS-LAS. We correct for this effect at $z < 0.1$ by extrapolating the light curve derived from a range of circular aperture magnitudes, as described in Section 2.2.

We then extrapolated this light curve out to the SDSS z -band Petrosian radius provided for each galaxy. In the NASA-Sloan Atlas (NSA), new and improved photometry is provided for SDSS galaxies at $z < 0.055$. In the case of galaxies in our sample that are included in the NSA catalog, we extrapolate to the new z -band Petrosian radius provided by the NSA.

At $z > 0.1$ the aperture clipping problem is minimal (see Figure 5). Given the nature of this study to investigate the possibility of a local ($z < 0.1$) under-density, we elected only to correct for aperture clipping at $z < 0.1$, to be as conservative as possible in the consideration of such a local under-density. As discussed in Section 2.4, we note that the application of this method has the effect of “correcting” the K -band galaxy counts from this sample (shown in Figure 6), such that they agree with previously published results from the literature.

While this method is rather crude, it allows for a means of estimating the light lost due to aperture clipping. We found that the median clipped aperture correction was ~ 0.1 magnitudes. We applied this method to all galaxies with clipped apertures down to 2 magnitudes below our selection limit for this study ($K < 16.3$). We found that this correction only increased the total number of galaxies in the sample by $\sim 0.25\%$ (via moving galaxies from fainter to brighter than the magnitude selection limit after the aperture correction).

2.3. Area Estimation

Given that we wish to investigate the surface density and volume density of various populations of galaxies, we need to know the area on the sky (and hence volume) of our survey. Due to the complex shape of the gaps and holes in this survey, a “by eye” determination of area would be tedious and unreliable. Instead, we employ a “counts-in-cells” method of determining area coverage. To do this, we first find the distance to the nearest neighbor on the sky for all objects in our catalog. Given the typical (median) nearest neighbor distance of $\delta \approx 150''$, we divide the entire area surveyed into square cells $\delta \times \delta$ in size.

From the center of each cell we tested a range of radii to search for nearby catalog objects. If catalog objects were detected within the search radius, then the cell was

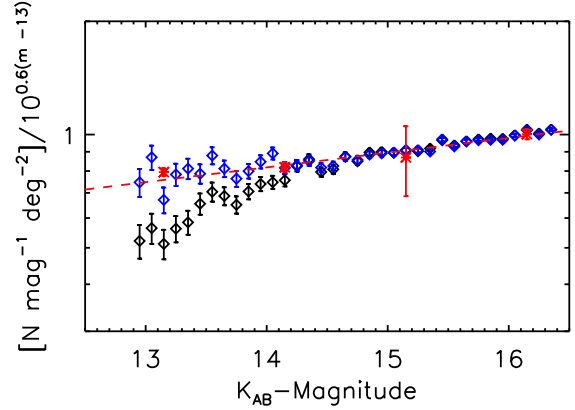


Figure 6. K -band galaxy counts as a function of apparent magnitude for this study compared with average K_s -band galaxy counts from Keenan et al. (2010b). The counts have been divided through by a normalized Euclidean model of slope $\alpha = 0.6$ to expand the ordinate (assuming the bright galaxy counts take the form $N(m) = A \times 10^{\alpha m}$, where A is a constant). Counts from Keenan et al. (2010b) are shown in red asterisks. Raw counts from this study are shown as black diamonds. Counts from this study after the aperture clipping correction was applied are shown in blue diamonds. These results indicate that the shape and normalization of K -band galaxy counts in this study are in good agreement with previous studies from the literature. This suggests that our area calculation is accurate, our star-galaxy separation is robust, and our aperture correction is having the desired effect. Note: we shift the Keenan et al. (2010b) K_s -band counts by $+0.15$ in magnitude to adjust for the typical magnitude difference for galaxies between K_s and the UKIDSS K -band filter following the results of Keenan et al. (2010b).

counted as surveyed area. We then simply count up the number of surveyed cells to compute the total area surveyed. We determined an optimal nearest-neighbor search radius of $300''$. Using this method we compute a total area for this work of 536.9 deg^2 on the sky. Varying our cell size and search radius by a factor of 2 was found to change our area estimate by only $\sim 2\%$. Thus, we estimate that our error in total area calculation is $\sim 2\%$. The exact estimate of the area is not critical to the results presented below, as it only serves to set the overall normalization.

2.4. Catalog Checks and Basic Analyses

The catalog generation methods described thus far yielded a catalog of 35,342 objects. Here we describe some of the basic consistency checks that we performed to verify that the final catalog was indeed what we intended it to be, namely, a K -band selected sample ($K < 16.3$) of all galaxies with NIR and optical photometry and spectroscopy where it existed.

As a fundamental check that we indeed have generated a magnitude limited sample of galaxies that is neither seriously contaminated by remaining stars nor plagued by the unintentional removal of a large number of galaxies in the catalog cuts, we turn to the galaxy counts as a function of apparent magnitude in our field. We compare our counts with those of Keenan et al. (2010b), who recently combined their deep wide-field NIR counts with data from the literature to come up with the best current estimate of average galaxy counts over a wide range in apparent magnitude.

The results of this comparison are shown in Figure 6. Black data points show the counts in our sample before the aperture clipping correction was applied. The aperture corrected counts are shown in blue, and we note that the counts for the aperture corrected data agree well with previous counts from the literature. These results suggest that our area estimation is accurate, our star-galaxy separation is robust, and our aperture correction method is appropriate.

2.5. Determination of Absolute Magnitudes

Ultimately, we wish to make a comparison of the rest-frame NIR luminosity density as a function of redshift. To do this, we need to adjust the observed apparent magnitudes in our sample by a distance modulus (DM), a $K(z)$ -correction to correct for bandpass shifting, and an evolution correction, $E(z)$, such that the absolute magnitudes used for constructing luminosity functions are given as:

$$M = m - DM(z) - K(z) + E(z). \quad (1)$$

At low redshifts in the NIR, $K(z)$ -corrections are nearly independent of galaxy type (Mannucci et al. 2001), allowing for this magnitude correction to be made without considering the type distribution of the galaxy sample. Combining SDSS and UKIDSS data, Chilingarian et al. (2010) showed that, at $z < 0.5$, accurate K -corrections can be calculated using low-order polynomials with input parameters of only the redshift and one observed NIR color. They have provided a K -correction calculator package⁹, which we used to compute K -corrections for galaxies in our sample. Chilingarian et al. (2010) compared their K -correction calculator output values with those obtained via the more rigorous spectral energy distribution fitting methods of Blanton & Roweis (2007) and Fioc & Rocca-Volmerange (1997) and concluded that the magnitude errors associated with K -corrections derived using their algorithm should be < 0.1 magnitudes.

Evolution of the rest-frame NIR light from galaxies is expected to be significantly weaker than in optical bandpasses (Blanton et al. 2003), but it is an effect that must be accounted for when comparing galaxy luminosities at different redshifts. A commonly assumed form of the evolution correction is $E(z) = Qz$, where Q is a positive constant. Blanton et al. (2003) showed that in the NIR, $Q = 1$ agrees well with stellar population synthesis models. Thus, for this study, we adopt $Q = 1$, such that $E(z) = z$. We further discuss this evolution correction, and its associated uncertainties, in Section 3.4.1.

3. THE K -BAND GALAXY LUMINOSITY FUNCTION

A number of different methods exist for estimating the galaxy LF. For an excellent review of the subject, we refer the reader to Johnston (2011). The most commonly assumed form of the LF is that of the Schechter (1976) function

$$\Phi(L)dL = \phi^* \left(\frac{L}{L_*} \right)^\alpha \exp \left(\frac{-L}{L_*} \right) \frac{dL}{L_*}, \quad (2)$$

which may be written in terms of absolute magnitudes using

⁹ <http://kcor.sai.msu.ru/>

$$\frac{L}{L_*} = 10^{-0.4(M - M^*)}, \quad (3)$$

giving

$$\Phi(M) = 0.4 \ln(10) \phi^* \frac{\left(10^{0.4(M^* - M)} \right)^{(\alpha+1)}}{\exp(10^{0.4(M^* - M)})}. \quad (4)$$

The Schechter function parameter L_* (or M^*) represents the luminosity of galaxies at the knee of the LF. ϕ^* determines the number density of L_* galaxies, and α is the faint-end slope. While the Schechter function has been demonstrated to provide a less-than-perfect fit to real data (e.g., Jones et al. 2006), it can provide a reasonably good fit and is the most widely used functional form for fitting the LF, making it the most useful form to consider when comparing with other studies from the literature.

To fit Schechter functions to observed data, a variety of methods have been used in the past. In Keenan et al. (2012), we compared four different LF estimators ($1/V_{\max}$, C^- , STY, and SWML) in the determination of NIR LFs. We found that the STY (Sandage et al. 1979) and SWML (Step-Wise Maximum Likelihood, Efstathiou et al. 1988) methods yielded similar results in the determination of M^* and α , while the C^- (Lynden-Bell 1971) and $1/V_{\max}$ (Schmidt 1968) methods tended to underestimate the faint end slope (see also Page & Carrera 2000). Of these four methods, $1/V_{\max}$ is the only one that provides the normalization (ϕ^*). In Keenan et al. (2012), we tested the $1/V_{\max}$ method alongside three other normalization estimators from Davis & Huchra (1982). We found all four of these estimators yielded consistent results, a confirmation of the same result found by Willmer (1997) using simulated data.

Given these analyses, in Keenan et al. (2012), we settled on a hybrid method to estimate the LF by first using STY to calculate M^* and α , and then using $1/V_{\max}$ (with M^* and α fixed) to determine the normalization. Here we use this same hybrid method in the determination of the K -band LF. To correct for spectroscopic incompleteness, we use a simple scheme in which each galaxy counted in the $1/V_{\max}$ procedure is weighted by a factor of $1/C(m)$, where $C(m)$ is the fractional completeness as a function of apparent magnitude.

3.1. The Assumption of a Constant LF Shape

In what follows, we make the critical assumption that the $z = 0$ shape parameters of the K -band LF (M^* and α) are not changing as a function of environment or distance from us. We require this assumption to facilitate the measurement of the K -band luminosity density as a function of redshift over this range. This is due to the fact that, in this sample, we have little or no information about the faint end slope of the LF at higher redshifts due to the magnitude limit of the survey, and we have corrupted information about the bright end of the LF at lower redshifts due to the Petrosian aperture clipping issue described in Section 2.2.

We believe the assumption of a constant LF shape is reasonable, given that the $K(z)$ -corrections are es-

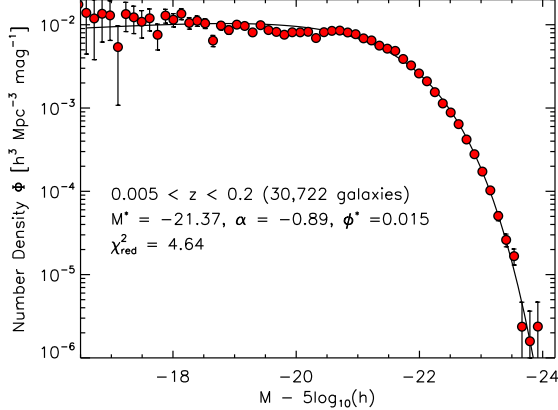


Figure 7. The UKIDSS-LAS K -band luminosity function over the range $0.005 < z < 0.2$. The red circles show the $1/V_{\max}$ LF estimate for this redshift range. Error bars show Poisson counting errors. The black curve shows the best fit normalization, $\phi^* = 0.015$, to $1/V_{\max}$ data after having determined the values of $M^* = -21.37$ and $\alpha = -0.89$ using the STY method. The value of $\chi^2_{\text{red}} = 4.64$ demonstrates the relatively poor fit of the Schechter function to the data.

entially independent of galaxy type and the $E(z)$ corrections are quite modest (see Section 2.5). Furthermore, De Propris & Christlein (2009) and Capozzi et al. (2012) have found that the shape of the NIR LF is not significantly different for field and cluster galaxies. Thus, in the following sections, we consider the K -band LF for all galaxies in our sample under the assumption that the shape of the $z = 0$ LF is not changing significantly as a function of distance from us or environment.

The assumption of a constant LF shape allows us to derive M^* using the higher redshift galaxies in the sample and then to determine the faint end slope, α , using the lower redshift galaxies. Thus, we used the STY method on the sample at redshifts $0.09 < z < 0.2$ to determine M^* with α fixed. We then used STY on the sample at $0.005 < z < 0.07$ to determine α with M^* fixed at the value determined using the higher redshift sample. We iterated this process until we reached convergence in the values of M^* and α . With M^* and α fixed, we then investigated the changing normalization (and hence changing luminosity density) as a function of redshift.

3.2. The K -band luminosity density at $0.005 < z < 0.2$

In Figure 7, we show the K -band LF for all galaxies in the redshift range $0.005 < z < 0.2$. The red circles show the $1/V_{\max}$ estimate of the LF, and the black curve shows a fit to these data having determined M^* and α using STY and then fitting ϕ^* to the $1/V_{\max}$ data. We note the poor fit to the data ($\chi^2_{\text{red}} = 4.6$). A poor fit of the Schechter function to LF estimates is not uncommon in studies from the literature (see e.g., Lavaux & Hudson 2011; Smith et al. 2009), and authors normally attribute this to the Schechter function being a poor model of the LF. However, in the analysis that follows we demonstrate that much of this fitting error may arise from density variations along the line of sight, and that in smaller redshift bins, the Schechter function provides a reasonable fit to the data.

It is worth noting at this point that a considerable por-

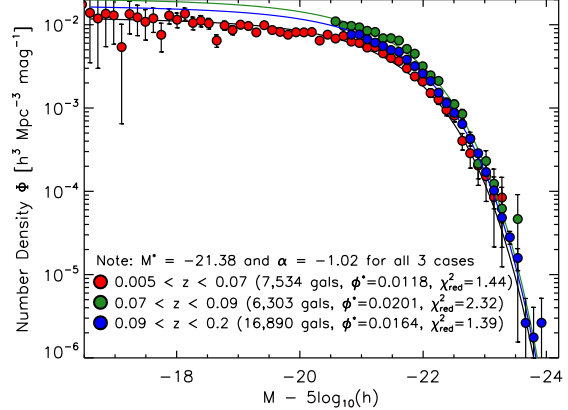


Figure 8. The UKIDSS-LAS K -band luminosity function split into three redshift ranges: $0.005 < z < 0.07$ (red), $0.07 < z < 0.09$ (green), and $0.09 < z < 0.15$ (blue). We separate the redshift range $0.07 < z < 0.09$ to demonstrate that the excess at $z > 0.09$ is not due to the Sloan Great Wall or the other over-densities we observe at higher declination in this redshift range. Here we have determined the LF shape parameters ($\alpha = -1.02$ and $M^* = -21.38$) iteratively using STY on both the high and low-redshift samples as described in Section 3.1. We then fit ϕ^* in each redshift range with α and M^* fixed. We list the χ^2_{red} values for each redshift range in the figure, and note that relatively good fits can be obtained using fixed LF shape parameters and letting the normalization (ϕ^*) vary as a function of redshift. We attribute the poor fit at $0.07 < z < 0.09$ to the large inhomogeneities in this range. However, this redshift bin was not used in the determination of the LF shape. As a result of these analyses, we find a value for ϕ^* that is ~ 1.4 times higher at $0.09 < z < 0.15$ than at $0.005 < z < 0.07$, suggesting a relative luminosity density that is high by the same factor. Error bars represent Poisson counting errors.

tion ($\sim 25\%$) of the solid angle subtended on the sky by this sample is filled by the Sloan Great Wall (Gott et al. 2005) at redshifts of $0.07 < z < 0.09$. In our sample, $\sim 40\%$ of the galaxies in this redshift range are part of this structure. The relative excess in the redshift distribution due to the Sloan Great Wall can be seen as a peak at these redshifts in Figure 3, both in the overall redshift distribution and, more prominently, in subregion 2, which is centered on this structure. Such structures will certainly be expected to cause some deformity in the LF, given that different luminosity ranges are preferentially sampled at different redshifts in an apparent magnitude limited survey.

In the same sense, it is worth noting that in Figure 7, the faint end of the LF is predominantly coming from the low-redshift end of the sample, and the bright end of the LF is mainly coming from the higher redshifts. With this in mind, in Figure 8, we show the LF for low-redshift galaxies in the range $0.005 < z < 0.07$ as red circles, the LF for the redshift range $0.07 < z < 0.09$ as green circles, and the LF for galaxies at $0.09 < z < 0.2$ as blue circles. The LF shape parameters, M^* and α , are the same for all three LFs shown in this figure. We determined M^* and α iteratively using the STY method by fitting M^* on the high-redshift ($0.09 < z < 0.2$) sample with α fixed, then fitting α on the low-redshift ($0.005 < z < 0.07$) sample with M^* fixed. We repeated this procedure until we reached convergence at values of $M^* = -21.38 \pm 0.04$ and $\alpha = -1.02 \pm 0.03$.

With M^* and α fixed, we fit the normalization, ϕ^* , to the LF estimate given by the $1/V_{\max}$ method. We

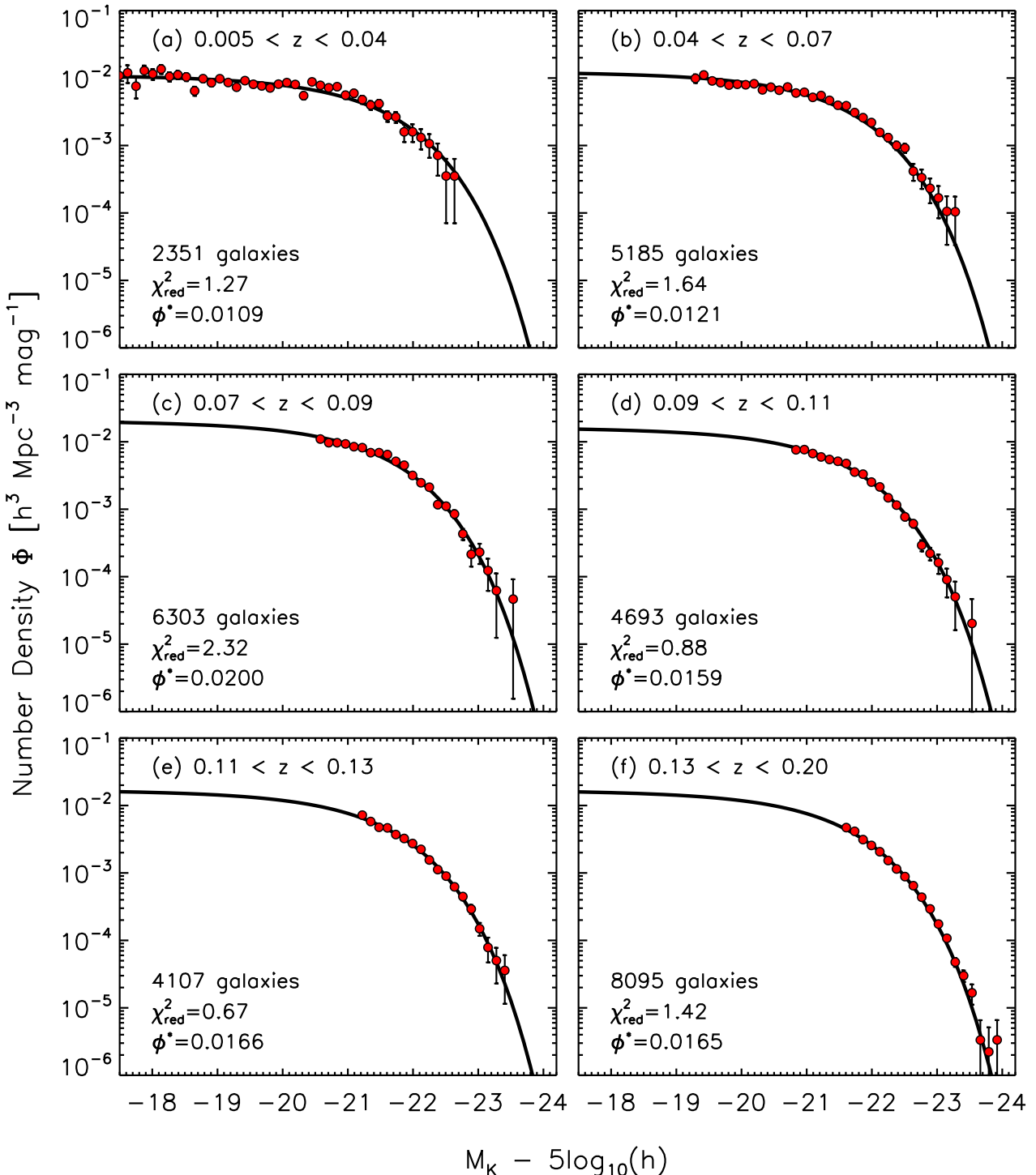


Figure 9. UKIDSS-LAS K -band LFs as a function of redshift. Here we have fixed the LF shape parameters ($\alpha = -1.02$ and $M^* = -21.38$) to those derived from the iterative fitting method described in Section 3.1 using the data presented in Figure 8. We then divided the sample into the six independent redshift bins shown here. In each case, the error bars show Poisson counting errors. We find that we can get a relatively good fit over all redshift bins (with the notable exception of the $0.07 < z < 0.09$ bin containing the Sloan Great Wall) by simply letting the Schechter function normalization vary as a function of redshift. The normalization (ϕ^*) and number of galaxies used to determine the LF in each bin are listed in the plots, as well as the χ^2_{red} values for each case.

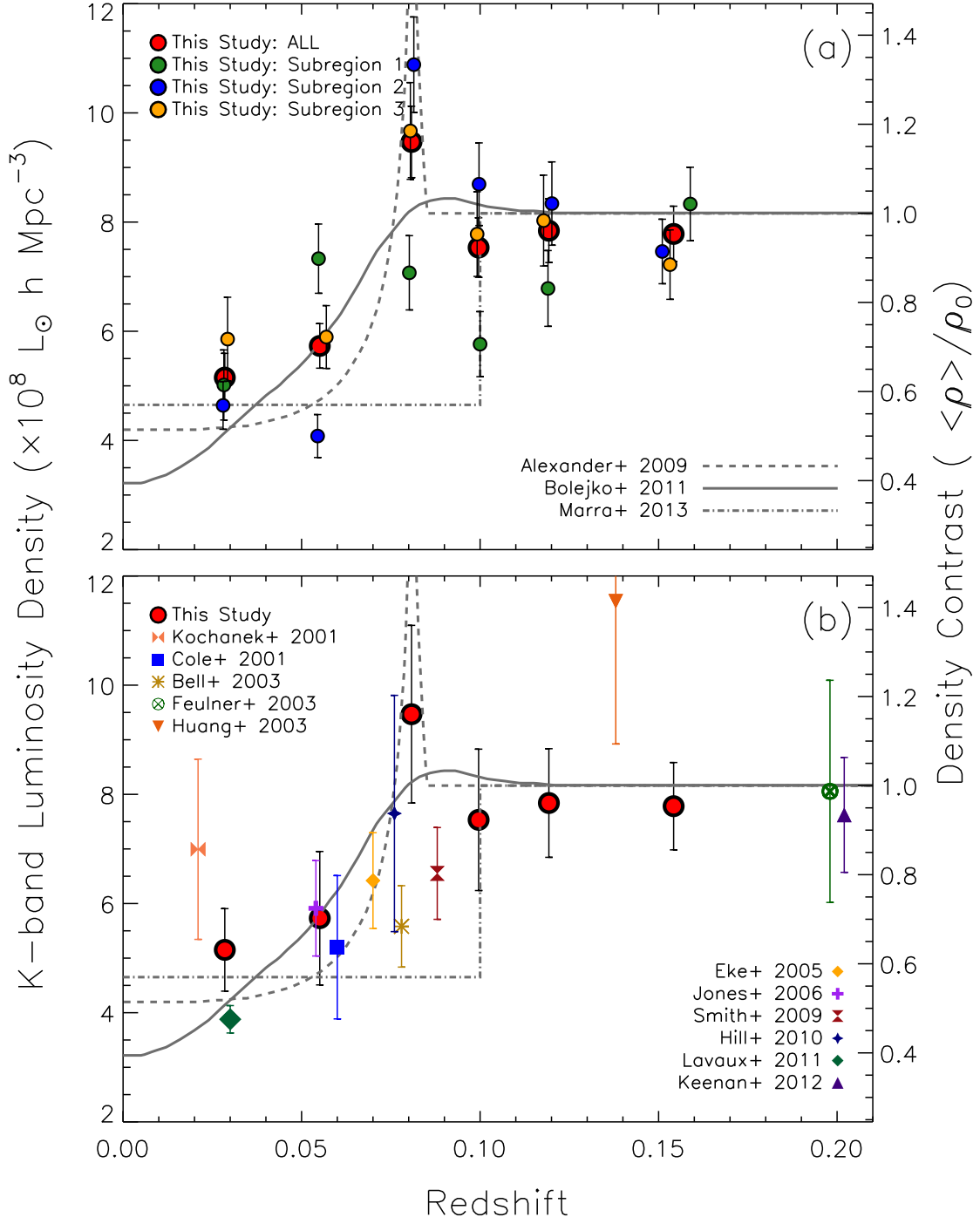


Figure 10. UKIDSS-LAS K -band luminosity density as a function of redshift. (a) Our measured K -band luminosity density for the full sample (red circles) versus different directions on the sky (green, blue, and orange circles corresponding to subregions 1, 2, and 3, respectively, in Figure 1). (b) Our measured K -band luminosity density for the full sample (red circles) as a function of redshift compared with other studies from the literature. The luminosity density for studies from the literature have been recalculated here using a consistent $M_{\odot, K}$ and Schechter function integration limits in all cases. The error bars on the data from this study in panel (b) represent the 1σ statistical errors in luminosity density in each bin combined with the systematic errors due to cosmic variance estimated from panel (a) of this plot. The density contrast, $\langle \rho \rangle / \rho_0$, is displayed on the right-hand vertical axis. The scale of the right-hand axis was established by performing an error-weighted least-squares fit (for the normalization only, not shape) of the void radial density profile of Bolejko & Sussman (2011) (gray solid curve) to all the luminosity density data in panel (b). The dashed curve shows the void radial density profile of Alexander et al. (2009). Both Alexander et al. (2009) and Bolejko & Sussman (2011) claim these density profiles can provide for good fits to the SNIa data without dark energy. The dash-dot curve shows the scale and amplitude of the ‘‘Hubble bubble’’ type perturbation that Marra et al. (2013) would require to explain the discrepancy between local measurements of the Hubble constant and those inferred by Planck. While all of the models shown for comparison are essentially toy models, they demonstrate the rough size scale of the under-densities considered in current minimal-void cosmological models.

Table 1
NIR luminosity densities and Schechter functions parameters for this study and selections from the literature

	$\langle z \rangle^a$	Redshift Range	N_{gals}	$M^*{}^b$	α	$\phi^*{}^c \times 10^3$	$j_{K, \text{calc}}{}^d$	$j_{K, \text{pub}}{}^e$
This Study	0.028	$0.005 < z < 0.04$	2,351	-21.38 ± 0.04	-1.02 ± 0.03	10.9 ± 0.5	$5.15 \pm 0.44(\pm 0.31)$	—
This Study	0.055	$0.04 < z < 0.70$	5,185	-21.38 ± 0.04	-1.02 ± 0.03	12.1 ± 0.6	$5.73 \pm 0.41(\pm 0.81)$	—
This Study	0.081	$0.07 < z < 0.09$	6,303	-21.38 ± 0.04	-1.02 ± 0.03	20.1 ± 0.8	$9.47 \pm 0.65(\pm 0.97)$	—
This Study	0.099	$0.09 < z < 0.11$	4,693	-21.38 ± 0.04	-1.02 ± 0.03	16.0 ± 0.4	$7.53 \pm 0.55(\pm 0.75)$	—
This Study	0.119	$0.11 < z < 0.13$	4,107	-21.38 ± 0.04	-1.02 ± 0.03	16.6 ± 0.5	$7.84 \pm 0.58(\pm 0.41)$	—
This Study	0.154	$0.13 < z < 0.20$	8,095	-21.38 ± 0.04	-1.02 ± 0.03	16.5 ± 0.4	$7.83 \pm 0.51(\pm 0.29)$	—
Keenan+ (2012)	0.200	$0.10 < z < 0.30$	812	-21.56 ± 0.06	-0.91 ± 0.07	14.6 ± 1.7	7.48 ± 1.03	—
Lavaux+ (2011)	0.030	$0.017 < z < 0.067$	60,000	-21.33 ± 0.02	-0.73 ± 0.02	11.1 ± 0.2	3.81 ± 0.25	(3.94 ± 0.02)
Hill+ (2010)	0.076	$0.003 < z < 0.1$	1,785	-21.66 ± 0.10	-0.96 ± 0.06	15.6 ± 1.6	7.65 ± 2.16	(6.98 ± 1.62)
Smith+ (2009)	0.100	$0.01 < z < 0.3$	40,111	-21.48 ± 0.04	-0.81 ± 0.04	16.6 ± 0.8	6.55 ± 0.84	(6.18 ± 0.07)
Jones+ (2006)	0.054	$0.0025 < z < 0.15$	60,869	-21.98 ± 0.03	-1.16 ± 0.04	7.5 ± 0.5	5.80 ± 0.85	(5.80 ± 0.50)
Eke+ (2005)	0.070	$0.005 < z < 0.12$	15,644	-21.58 ± 0.04	-0.81 ± 0.07	14.3 ± 0.8	6.30 ± 0.86	(7.04 ± 0.23)
Bell+ (2003)	0.078	$0.0033 < z < 0.2$	6,282	-21.44 ± 0.05	-0.77 ± 0.04	14.3 ± 0.7	5.48 ± 0.73	(5.80 ± 1.80)
Huang+ (2003)	0.138	$0.005 < z < 0.35$	1,056	-21.85 ± 0.08	-1.37 ± 0.10	13.0 ± 3.0	11.32 ± 2.56	—
Feulner+ (2003)	0.200	$0.10 < z < 0.30$	210	-21.94 ± 0.24	-1.10 ± 0.10	11.1 ± 1.2	7.91 ± 2.00	—
Cole+ (2001)	0.060	$0.023 < z < 0.12$	5,683	-21.59 ± 0.03	-0.96 ± 0.06	10.8 ± 1.6	5.10 ± 1.29	(5.74 ± 0.86)
Kochanek+ (2001)	0.023	$0.007 < z < 0.1$	3,878	-21.54 ± 0.05	-1.09 ± 0.06	11.6 ± 1.0	6.87 ± 1.62	(7.14 ± 0.75)

^a The mean redshift values listed for this study are averages for each redshift bin. In other studies the value in this column is not strictly a mean, but rather, whatever the authors listed (mean or median) or our own estimate if no value was given in the original article.

^b M^* values are given as $M - 5\log_{10}(h)$. Note, these are the published values, however, in calculating the luminosity density we adjusted studies using UKIDSS K -band Petrosian magnitudes (this study, Smith et al. 2009, Hill et al. 2010) to 0.15 mags brighter in M^* for consistency with 2MASS “total” K_s -band magnitudes.

^c ϕ^* values are given in units of $h^3 \text{ Mpc}^{-3}$.

^d K -band luminosity density in units of $10^8 L_{\odot} h \text{ Mpc}^{-3}$. These are the values used in Figure 10 for which we have calculated j_K such that all studies are assuming the same value for $M_{\odot, K}$ and the same limits of integration of the Schechter function. The errors listed for this study are first statistical errors followed by an estimate of cosmic variance error in parentheses.

^e K -band luminosity density as published in the studies listed. These values differ from those we calculate ourselves primarily due to different assumptions of the value of $M_{\odot, K}$.

find that the LFs for the high-redshift and low-redshift samples shown in Figure 8 can be reasonably well fit by the same M^* and α parameters, while only allowing the normalization to change (we attribute the comparably poor fit at $0.07 < z < 0.09$ to the large inhomogeneities in this redshift bin). This indicates that the assumption of a constant LF shape as a function of redshift and environment appears to be valid. As shown in Figure 8, we find a normalization at $0.09 < z < 0.2$ that is ~ 1.4 times higher than that at $0.005 < z < 0.07$. Thus, if the LF shape is indeed constant for this sample, then the luminosity density at $z > 0.09$ appears to be ~ 1.4 times higher than that at $z < 0.07$, even when known over-densities at $0.07 < z < 0.09$ are excluded.

Next, we investigated the K -band luminosity density as a function of redshift in a series of narrower redshift bins over the range $0.005 < z < 0.2$, as labeled in each panel of Figure 9. We fixed the LF shape parameters to the values derived above ($\alpha = -1.02$ and $M^* = -21.38$) and fit the normalization to the $1/V_{\text{max}}$ results in each redshift bin. Red circles show the $1/V_{\text{max}}$ results in each case, and the black solid curves represent the Schechter function fits. Again, we find that the data in all of the redshift bins are reasonably well fit with the same M^* and α parameters ($\chi^2_{\text{red}} \sim 1$ except at $0.07 < z < 0.09$), suggesting that the assumption of a constant LF shape is valid. We also note in each panel the measured value for ϕ^* and the number of galaxies used to generate the LF.

3.3. Comparison With Studies From the Literature

In Figure 10, we use the results from Figure 9 to calculate the K -band luminosity density as a function of redshift (by integrating the fitted Schechter functions). In Figure 10a we show how these results vary as a function

of position on the sky by comparing the average result for the full sample (red circles) with the results from each of the three subsamples (green, blue, and orange circles) of galaxies from the subregions shown in Figure 1. Each of these subsamples contains roughly a third of the original sample of galaxies. While we find stark differences between subsamples in the measured luminosity density in some redshift bins, the overall trend toward a rising luminosity density with increasing redshift appears present in all cases. We use the rms variation in luminosity density in each redshift bin as an estimate of the systematic error due to cosmic variance in our measurement. These systematics are reflected in the larger error bars for the total sample in Figure 10b.

In Figure 10b, we compare our results with other studies from the literature, where red circles again show our results for the entire sample, and studies from the literature correspond to the symbols listed in the plot legend. The luminosity densities presented in this figure for studies from the literature have been recalculated here using the same value for $M_{\odot, K}$ and Schechter function integration limits in all cases for consistency. All the data displayed here are listed in Table 1. The majority of studies at $z < 0.1$ have used photometry from the Two Micron All Sky Survey (2MASS, Jarrett et al. 2000). These studies have typically used the 2MASS K_s -band ($2.12\mu\text{m}$) Kron or “total” magnitudes which are generally found to be ~ 0.15 mags brighter than UKIDSS K -band Petrosian magnitudes (see e.g., Keenan et al. 2010a; Smith et al. 2009). Thus, in making this comparison, we have adjusted the values for M^* to be 0.15 mags brighter for our study and other studies derived from UKIDSS data (Hill et al. 2010; Smith et al. 2009). Making this adjustment does not change the results presented here, but is done for the sake of consistency. In

general, we find excellent agreement with all previously published results in the K -band, and we confirm the tentative result presented in Keenan et al. (2012) of a rising luminosity density from $z \approx 0.05$ to $z \approx 0.1$, which appears to remain higher than that measured locally out to $z \sim 0.2$.

The relative density contrast, $\langle \rho \rangle / \rho_0$, is displayed on the right-hand vertical axis in Figure 10. The scale of this axis was established by performing an error-weighted least-squares fit of the void radial density profile of Bolejko & Sussman (2011) (solid curve, fitting only the normalization only, not the shape) to all the luminosity density data in panel (b). As mentioned in Section 1, this means we are assuming a linear bias parameter of $b = 1$, or more specifically that K -band luminosity density is an unbiased tracer of the underlying dark matter density. We believe this is a reasonable assumption given previous results from observations and simulations (e.g., Maller et al. 2005; Angulo et al. 2013).

The dashed curve in Figure 10 shows the void radial density profile of Alexander et al. (2009), also normalized to a density contrast of unity at high redshift. Both Alexander et al. (2009) and Bolejko & Sussman (2011) claim these density profiles allow for a good fit to the SNIa data without dark energy. The dash-dot curve shows the scale and amplitude of the “Hubble bubble” type perturbation that Marra et al. (2013) would require to explain the discrepancy between local measurements of the Hubble constant and those inferred by Planck. While all three of these models are essentially toy models, they demonstrate the rough size scale of the underdensities considered in current minimal-void cosmological models.

In general, the data from this study and those from the literature seem to indicate a rising luminosity density out to $z \sim 0.1$. The notable exception to this trend would be the measurement of Kochanek et al. (2001). However, we note that the relatively low luminosity density found by Lavaux & Hudson (2011) is also derived from 2MASS, but with much improved photometry, and includes a sample more than an order of magnitude larger, which itself contains the original sample from Kochanek et al. (2001).

The studies of Cole et al. (2001), Bell et al. (2003), Eke et al. (2005), and Jones et al. (2006) are also based on 2MASS photometry, and all agree well on a significantly higher value for the luminosity density than that found by Lavaux & Hudson (2011). However, all four of these studies considered deeper redshift samples extending to $z > 0.1$. Qualitatively speaking, in all four cases a tension similar to that which we show in Figure 7, between the observed LF and the best Schechter function fit, appears present. This phenomenon is seen most dramatically in the work of Jones et al. (2006), where they display the residuals of their Schechter fits to the LF showing that the faint end is overestimated by the fit, while there appears to be an excess of galaxies around $M \sim M^*$. We would argue, based on our own study of the LF, that much of the irregularity in the LF shape found by these studies may be due to inhomogeneity along the line of sight, and more specifically, to a higher space density of galaxies at the high-redshift end of the samples.

Hill et al. (2010) use UKIDSS data to measure the

K -band luminosity density in the field targeted by the Millennium Galaxy Catalog Survey (Dec = $0, 10^h < \text{RA} < 15^h$, Liske et al. 2003). As noted in Section 3.2, this region contains the Sloan Great Wall. Hill et al. (2010) correct for this over-density by adjusting their normalization down by $\sim 20\%$. Undoing this correction would bring their measurement into good agreement with our result at roughly the same redshift.

The sample of Smith et al. (2009) is the most similar to our own. They select $\sim 40,000$ galaxies from the UKIDSS-LAS with redshifts from the SDSS. They measure the LF for the entire sample from $0.01 < z < 0.3$. They find similar irregularities in the LF shape to those we present in Figure 7. They note that when they divide their sample into three redshift bins they see a rising LF normalization with increasing redshift, and point out that even doubling their evolution correction does not resolve this issue.

The sample sizes of Huang et al. (2003), Feulner et al. (2003), and Keenan et al. (2012) are generally too small to be considered robust to cosmic variance. However, it is worth noting that the measurements of Feulner et al. (2003) and Keenan et al. (2012) may be considered conservative underestimates of the true luminosity density because these studies avoided known over-densities, such as galaxy clusters, in the redshift ranges sampled.

We conclude that if the observed trend in K -band luminosity density as a function of redshift is indicative of a similar trend in the underlying total mass density, then the local universe may be under-dense on a scale and amplitude sufficient to introduce significant biases into local measurements of cosmological observables. Leaving aside considerations of whether or not such an unusual local structure could obviate the need for dark energy, given the analysis of Marra et al. (2013), it appears that the observed under-density is roughly the right scale and amplitude to explain the apparent tension between local measurements of the Hubble constant ($H_0 = 73.8 \pm 2.4 \text{ km s}^{-1} \text{ Mpc}^{-1}$, Riess et al. 2011) and the recent results from Planck ($H_0 = 67.3 \pm 1.2 \text{ km s}^{-1} \text{ Mpc}^{-1}$, Planck Collaboration et al. 2013).

3.4. Possible Sources of Bias and Error in This Measurement

We have done everything possible in this study to make an unbiased measurement of the K -band luminosity density as a function of redshift in the nearby universe. However, we are pushing the data by making several assumptions that allow us to probe a wider redshift range than that for which we have a statistically robust measurement of the LF over the entire range of absolute magnitudes. Here we discuss the possible biases and errors in our measurement associated with these assumptions.

3.4.1. $K(z)$ and $E(z)$ corrections

The most important assumption we make in this study is that the $z = 0$ shape of the K -band LF is not changing significantly as a function of distance from us. This, in turn, relies on the assumption that we are making the appropriate $K(z)$ and $E(z)$ corrections to calculate the $z = 0$ absolute magnitudes of galaxies at any given redshift. To investigate these assumptions in detail, we explored variations in the $K(z)$ and $E(z)$ corrections to see how they affect our result.

If we simply omit the $K(z)$ -corrections in our calculations, we find that the excess luminosity density at $z > 0.1$ shown in Figure 10 increases significantly (due to the fact that the K -correction is negative). We compared the K -correction calculator outputs of Chilingarian et al. (2010) to the empirical estimates by Mannucci et al. (2001) and found qualitative agreement, but on average the K -corrections of Mannucci et al. (2001) are ~ 0.1 mags more negative than the calculator outputs. We ran all of our analyses using the average K -corrections of Mannucci et al. (2001) and found that the excess luminosity density at $z > 0.1$ is reduced slightly, but not significantly. In general, we expect the calculator outputs to be more robust estimates of the true K -corrections as they were derived using a much larger sample than that of Mannucci et al. (2001), and the sample was drawn from the UKIDSS and SDSS surveys, which we use for this study.

The $E(z)$ corrections we use are of the form $E(z) = Qz$, as described in Section 2.5, and also act to slightly reduce the observed excess in luminosity density. To explore the possibility of underestimated evolution, we increased the Q parameter arbitrarily to investigate the effects of stronger evolution. We found we needed to increase the evolution correction to $Q = 4$ to make the average luminosity density at $z > 0.1$ roughly equal to that at $z = 0.05$. This would imply that galaxies are dimming by $\sim 30\%$ in the rest-frame K -band over the last 1–2 Gyrs. This amount of evolution would require galaxies to form at $z \ll 1$, which is ruled out by galaxy star formation histories. Thus, we do not expect underestimates of the $E(z)$ corrections to be a possible source of the excess luminosity density at $z > 0.1$.

3.4.2. The Faint-end Slope of the Luminosity Function

At $z > 0.1$ we are not making a robust estimate of the faint end slope (α) of the LF. We examined the possibility that a less negative slope than that measured at $z < 0.07$ (i.e., $\alpha < -1.02$) at $z > 0.1$ could account for the observed excess in luminosity density. This is, essentially, another means of exploring the possible effects of unanticipated evolution in the LF as a function of redshift. We found that a slope of $\alpha \approx -0.65$ imposed at $z > 0.1$ (while leaving $\alpha = -1.02$ at $z < 0.07$) was sufficient to suppress the observed excess at $z > 0.1$. However, this would not explain the rising normalization with increasing redshift. In addition, the vast majority of studies of the NIR LF from the literature measure α to be $\sim 0.9 - 1.1$ for $0 < z < 0.3$ (e.g., Cole et al. 2001; Kochanek et al. 2001; Feulner et al. 2003; Jones et al. 2006; Hill et al. 2010). Thus, $\alpha = -0.65$ at $z > 0.1$ would not only represent some kind of extreme evolution in the LF but also be at odds with results from the literature. Therefore, we do not consider this to be a reasonable candidate for the observed excess luminosity density at $z > 0.1$.

3.4.3. Spectroscopic Selection Bias

The spectroscopy for this study comes mainly from the SDSS and is supplemented by other published redshift surveys. Targets for SDSS spectroscopy were chosen using an R -band selection, and, in general, the targets for other redshift surveys from the literature were also selected optically. Thus, there could exist a bias in the

spectroscopic redshift distribution for a K -band selected sample for which spectroscopic targets have been selected in optical bands. At $z \sim 0.05$, the typical $R - K$ color of galaxies is ~ 2 , while at $z \sim 0.15$, $R - K \sim 1.25$. Thus, there will be a bias against faint K -selected sources at low redshifts being chosen for spectroscopic follow-up in an R -band target selection (relative to the same selection at higher redshifts). In principle, such a selection bias could reduce the overall K -band LF normalization at low redshifts.

For this reason, we restrict this study to only areas of very high spectroscopic completeness. The minimum acceptable completeness for regions covered in this study is 90%, and, on average, the completeness is $\sim 95\%$ at $K_{\text{AB}} < 16.3$. To estimate the limiting case of the $R - K$ spectroscopic selection bias, we consider the extreme scenario in which all galaxies lacking spectroscopy are assumed to reside at $z < 0.07$. In this case, we estimate that the LF normalization at $z < 0.07$ could be increased by as much as $\sim 20\%$.

However, the median apparent K -band magnitude of a galaxy at $z < 0.07$ is roughly 0.75 mags brighter than that of a galaxy at $z > 0.09$ in this study, so the spectroscopic selection effect should be essentially cancelled out by the fact that nearby galaxies are intrinsically brighter on the sky, and we would expect any biases due to such selection effects at low redshifts to be much smaller than the 20% quoted above.

If we assume that spectroscopic selection bias is not a problem in this study, then we can expand the area on the sky to include the entire region of overlap between the UKDISS-LAS and the SDSS. In doing so, the average overall completeness of the sample drops to $\sim 85\%$, but the volume is increased by roughly a factor of four (increase in area from $\sim 500 \text{ deg}^2$ to $\sim 2000 \text{ deg}^2$). We performed all of the analyses described above on this full sample of $\sim 140,000$ galaxies and obtained very similar results, namely, that the K -band luminosity density at $z > 0.1$ appears to be ~ 1.5 times higher than that measured locally.

3.4.4. Photometric Errors

As noted in Section 2.2, galaxies which subtend a large solid angle on the sky may have their Petrosian fluxes underestimated due to the upper limit of $6''$ (corresponding to a $12''$ circular aperture radius) on the size of the Petrosian aperture in the WSA pipeline. As demonstrated in Figure 5, this issue presents a problem at low redshifts ($z < 0.1$) where a significant fraction of objects have had their Petrosian apertures clipped, and thus their fluxes underestimated.

In Section 2.2, we describe a method to estimate a flux correction for galaxies where the Petrosian aperture was clipped by using a range of circular aperture magnitudes to measure a light curve for each galaxy, and then extrapolating to the z -band Petrosian aperture radius given in the SDSS. We show in Figure 6 that making this correction brings the galaxy counts for our sample into agreement with the expected distribution taken from all-sky galaxy counts in the K -band. We explored the effect of arbitrarily increasing this correction and found that a larger correction (by a factor of ~ 2) had the effect of overpopulating the bright end of the galaxy counts distribution.

We found that applying the aperture clipping correction factor before making the initial apparent magnitude selection in the K –band only increased the sample size by $\sim 0.25\%$. Before making this aperture correction, we found that the bright end of the LF at low redshifts ($z < 0.05$) appeared to fall off more steeply than expected (given the distribution seen at slightly higher redshifts). Upon making the correction, the bright end of the LF at low redshifts was moved to brighter magnitudes and toward better agreement with higher redshift results.

We note, however, that in the lowest redshift bin presented in Figure 9, the bright end of the LF still appears to fall off more steeply than at higher redshifts. We found that arbitrarily increasing the aperture correction in this redshift bin appears to bring the bright end of the LF into better agreement with the LFs in higher redshift bins. Thus, we conclude that we are probably underestimating the aperture clipping correction at the very lowest redshifts. However, the aperture correction itself (even when increased arbitrarily) does almost nothing to increase the normalization of the LF. This is because intrinsically bright (large) galaxies are those most affected by aperture clipping, and correcting for this effect only shifts the bright end of the LF along the abscissa.

Thus, while this method represents a rather crude lost light correction for any individual galaxy, we believe that it provides a statistically sound means of recovering the galaxy luminosity distribution. Furthermore, we find that the relative distribution of K –band luminosity density as a function of redshift presented in Figure 10 is not significantly altered by making this correction (or doubling it for that matter).

3.4.5. Cosmic Variance

Systematic bias due to cosmic variance is a possible source of error in any measurement made over a volume that is insufficient to average over large-scale structure in the universe. As noted in Section 1, the largest structures observed in the local universe appear to be of order the size of the largest volumes surveyed to date. Thus, it remains unclear what the upper limit on the size of structure is and what volume constitutes a representative sample of the universe.

To address the issue of cosmic variance, we divided our sample into three subsamples denoted by the different regions on the sky shown in Figure 1. As shown in Figure 10, our measured luminosity density in some redshift bins varied dramatically among the three subsamples, but, in general, the overall trend toward a rising luminosity density with increasing redshift is present in all three regions on the sky.

In the highest redshift bins the results from the different subsamples appear to be converging, suggesting that some kind of ‘scale of homogeneity’ has been reached, but the substantial increase in luminosity density compared to the lowest redshift bins implies that structure may exist on scales larger than the survey volume. We estimate the systematics due to cosmic variance in each of our six redshift bins given the rms scatter between measurements from the three subregions. We present this error estimate in Table 1 and graphically in Figure 10b.

As a final check that our methods are sound, and to investigate further the expected effects of cosmic variance, we performed all the same analyses described above

to estimate the relative variation in K –band luminosity density as a function of redshift using mock catalogs from the Millennium database online¹⁰. The Millennium database contains a variety of mock catalogs based on the Millennium (Springel et al. 2005) and Millennium-II (Boylan-Kolchin et al. 2009) simulations. We used the ‘Blaizot2006’ all-sky catalogs, which were generated using the MoMaF code (Blaizot et al. 2005), as well as the ‘Henriques2012’ all-sky catalogs created using the visual observing algorithm of Henriques et al. (2012) and the semi-analytical model of Guo et al. (2011).

From both catalogs, we retrieved all-sky K –selected catalogs of galaxies at $K < 16.3$. We divided each all-sky catalog into 16 different regions to be considered independently. While each of these regions of ~ 2500 deg 2 is much larger than our observed sample, we expect the effects of cosmic variance to be similar, because our observed sample spans many widely separated fields on the sky. While it is difficult to quantify exactly how cosmic variance should scale in such a comparison, Driver & Robotham (2010) show that for a sample made up of N independent fields, cosmic variance should be reduced by a factor of $1/\sqrt{N}$.

We then computed the K –band luminosity density as a function of redshift for each of the 16 regions in both mock catalogs using the same methods as were used with the observed data, namely, applying the same $K(z)$ and $E(z)$ corrections and estimating the LF in the same way. In Figure 11, we show the results of this exercise, where blue circles represent the Henriques2012 mock catalog, and red circles represent the Blaizot2006 catalogs. The data points show the average result in each redshift bin, and all results are normalized to the average in the highest redshift bin. The error bars show the standard deviation of the distribution of measured luminosity densities in each redshift bin for the 16 regions considered in each catalog.

Thus, we find that a typical deviation of $\sim 10 - 20\%$ could be expected in this measurement between the lowest and highest redshift bins. While this result could be further quantified by including additional or independent realizations of mock catalogs, our interest here is simply to show that when we apply our methods to simulated catalogs, we recover the expected result that the K –band luminosity density is not changing dramatically as a function of redshift.

4. SUMMARY

We have presented a study of the K –band luminosity density in the redshift range $0.005 < z < 0.2$. This study is based on a K –band selection of galaxies taken from the UKIDSS-LAS, where spectroscopy from the SDSS and other redshift surveys provides for > 500 deg 2 on the sky that is $> 90\%$ spectroscopically complete to $K_{AB} < 16.3$. The primary motivation for this study is to explore the low-redshift stellar mass density distribution of the universe to test for the possibility that the nearby universe is under-dense on a scale and amplitude sufficient to introduce significant biases into locally measured cosmological observables. This work represents the first time that the NIR luminosity density has been measured

¹⁰ <http://gavo.mpa-garching.mpg.de/MyMillennium/>

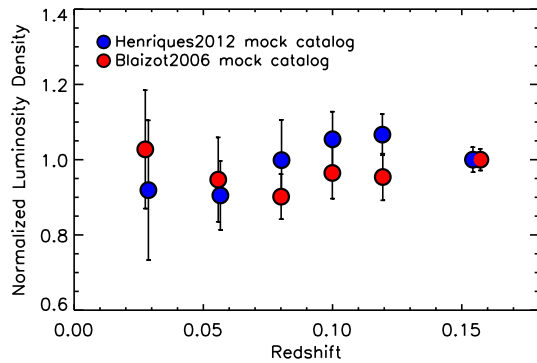


Figure 11. Normalized luminosity density in the K -band derived from two different mock catalogs using all the same methods as were used on the observed data. In each case, we divided the all sky catalog for the $K < 16.3$ sample into 16 sight lines, for which we calculated the luminosity density in each of the six redshift bins individually. The data points show the average result in each redshift bin for the Blaizot2006 catalogs (red circles) and the Henriques2012 catalog (blue circles). The error bars show the standard deviation of the results over the 16 sight lines in each redshift bin for both catalogs. The results are shown normalized to the average in the highest redshift bin.

in the nearby universe with consistent methods and photometry over a wide range in redshift.

We find that we can achieve good fits to the K -band galaxy LF both at low redshifts and at higher redshifts using the same LF shape parameters, M^* and α . We find values for these LF shape parameters of $M^* = -21.38 \pm 0.04$ and $\alpha = -1.02 \pm 0.03$ by iteratively fitting α on the low-redshift data while holding M^* fixed, then fitting M^* on the higher-redshift data while holding α fixed until convergence is achieved.

Next, we consider six redshift bins over the range $0.005 < z < 0.2$ to explore the K -band luminosity density as a function of redshift in detail. To do this, we fix M^* and α and only fit the normalization, ϕ^* , in each bin. We find excellent agreement with all previous measurements of the K -band LF from the literature. We confirm the tentative detection, presented in Keenan et al. (2012), of a rising NIR luminosity density over the range $0.005 < z < 0.1$ and a luminosity density at $z \sim 0.2$ that is ~ 1.5 times higher than that measured locally.

We also divide our sample into three subsamples to consider the issue of cosmic variance. We find that, while individual measurements of the luminosity density in a given redshift bin may differ by a factor of two between subregions, the overall trend with redshift is consistent between the subregions. At the highest redshifts considered in this sample, the measurement in the three subsamples appears to be converging on the result that the luminosity density at $z > 0.1$ appears to be ~ 1.5 times higher than that measured locally. In particular, it is worth noting that in subregions 1 and 2, which represent opposite directions on the sky, the measurements agree very well on the luminosity density in both the lowest and highest redshift bins. This relative agreement between widely separated sight lines, combined with the fact that the K -band galaxy counts from this study agree well with previously published all-sky galaxy counts, suggests that the phenomenon of a rising luminosity density with increasing distance from us may be a general trend in

the nearby universe. Given the analysis of Marra et al. (2013), we can say that such a scenario would be sufficient to explain the apparent tension between direct measurements of the Hubble constant and those recently published by the Planck collaboration.

As NIR luminosity is a good tracer of stellar mass, and stellar mass density should trace the underlying dark matter distribution, we compare our results with the void radial density profiles of Bolejko & Sussman (2011) and Alexander et al. (2009), which they claim could act to produce the apparent acceleration of the expansion of the universe observed via type Ia supernovae. While these void models are simplistic, they give a rough idea of the minimal scale and amplitude required for a local under-density to introduce significant biases in locally measured cosmological observables, such as the expansion rate. We conclude that local measurements of the NIR luminosity density could be described as consistent with cosmological models that invoke a large local under-density on radial scales of a few hundred Mpc to explain the apparent acceleration of the expansion of the universe.

We gratefully acknowledge support from the University of Wisconsin Research Committee with funds granted by the Wisconsin Alumni Research Foundation and the David and Lucile Packard Foundation (A. J. B.) and NSF grant AST-0709356 (L. L. C.).

This work is based in part on data products from the UKIRT Infrared Deep Sky Survey (UKIDSS).

This publication makes use of data products from the Sloan Digital Sky Survey (SDSS). Funding for the SDSS and SDSS-II has been provided by the Alfred P. Sloan Foundation, the Participating Institutions, the National Science Foundation, the U.S. Department of Energy, the National Aeronautics and Space Administration, the Japanese Monbukagakusho, the Max Planck Society, and the Higher Education Funding Council for England. The SDSS Web Site is <http://www.sdss.org/>. The SDSS is managed by the Astrophysical Research Consortium for the Participating Institutions. The Participating Institutions are the American Museum of Natural History, Astrophysical Institute Potsdam, University of Basel, University of Cambridge, Case Western Reserve University, University of Chicago, Drexel University, Fermilab, the Institute for Advanced Study, the Japan Participation Group, Johns Hopkins University, the Joint Institute for Nuclear Astrophysics, the Kavli Institute for Particle Astrophysics and Cosmology, the Korean Scientist Group, the Chinese Academy of Sciences (LAMOST), Los Alamos National Laboratory, the Max-Planck-Institute for Astronomy (MPIA), the Max-Planck-Institute for Astrophysics (MPA), New Mexico State University, Ohio State University, University of Pittsburgh, University of Portsmouth, Princeton University, the United States Naval Observatory, and the University of Washington.

This research made use of the “K-corrections calculator” service available at <http://kcor.sai.msu.ru/>.

This work has made use of NASA’s Astrophysics Data System.

REFERENCES

Alexander, S., Biswas, T., Notari, A., & Vaid, D. 2009, JCAP, 9, 25

Alnes, H., Amarzguioui, M., & Grøn, Ø. 2006, Phys. Rev. D, 73, 083519

Angulo, R. E., Hahn, O., & Abel, T. 2013, ArXiv e-prints

Bell, E. F., & de Jong, R. S. 2001, ApJ, 550, 212

Bell, E. F., McIntosh, D. H., Katz, N., & Weinberg, M. D. 2003, ApJS, 149, 289

Biswas, T., Notari, A., & Valkenburg, W. 2010, JCAP, 11, 30

Blaizot, J., Wadadekar, Y., Guiderdoni, B., Colombi, S. T., Bertin, E., Bouchet, F. R., Devriendt, J. E. G., & Hatton, S. 2005, MNRAS, 360, 159

Blanton, M. R., & Roweis, S. 2007, AJ, 133, 734

Blanton, M. R., et al. 2003, ApJ, 592, 819

Bolejko, K., Célérier, M.-N., & Krasiński, A. 2011, Classical and Quantum Gravity, 28, 164002

Bolejko, K., & Sussman, R. A. 2011, Physics Letters B, 697, 265

Boylan-Kolchin, M., Springel, V., White, S. D. M., Jenkins, A., & Lemson, G. 2009, MNRAS, 398, 1150

Bull, P., & Clifton, T. 2012, ArXiv e-prints

Busswell, G. S., Shanks, T., Frith, W. J., Outram, P. J., Metcalfe, N., & Fong, R. 2004, MNRAS, 354, 991

Capozzi, D., Collins, C. A., Stott, J. P., & Hilton, M. 2012, MNRAS, 419, 2821

Célérier, M.-N. 2000, A&A, 353, 63

Célérier, M.-N., Bolejko, K., & Krasiński, A. 2010, A&A, 518, A21

Chilingarian, I. V., Melchior, A.-L., & Zolotukhin, I. Y. 2010, MNRAS, 405, 1409

Chung, D. J. H., & Romano, A. E. 2006, Phys. Rev. D, 74, 103507

Clarkson, C. 2012, Comptes Rendus Physique, 13, 682

Clarkson, C., & Maartens, R. 2010, Classical and Quantum Gravity, 27, 124008

Cole, S., et al. 2001, MNRAS, 326, 255

Colless, M., et al. 2001, MNRAS, 328, 1039

Davis, M., & Huchra, J. 1982, ApJ, 254, 437

de Jong, R. S. 1996, A&A, 313, 377

De Propis, R., & Christlein, D. 2009, Astronomische Nachrichten, 330, 943

Driver, S. P., & Robotham, A. S. G. 2010, MNRAS, 407, 2131

Efstathiou, G., Ellis, R. S., & Peterson, B. A. 1988, MNRAS, 232, 431

Eke, V. R., Baugh, C. M., Cole, S., Frenk, C. S., King, H. M., & Peacock, J. A. 2005, MNRAS, 362, 1233

Enqvist, K., & Mattsson, T. 2007, JCAP, 2, 19

February, S., Larena, J., Smith, M., & Clarkson, C. 2010, MNRAS, 405, 2231

Feulner, G., Bender, R., Drory, N., Hopp, U., Snigula, J., & Hill, G. J. 2003, MNRAS, 342, 605

Fioc, M., & Rocca-Volmerange, B. 1997, A&A, 326, 950

Frith, W. J., Busswell, G. S., Fong, R., Metcalfe, N., & Shanks, T. 2003, MNRAS, 345, 1049

Frith, W. J., Shanks, T., & Outram, P. J. 2005, MNRAS, 361, 701

García-Bellido, J., & Haugbølle, T. 2008, JCAP, 4, 3

García-Bellido, J., & Haugbølle, T. 2008, JCAP, 9, 16

—. 2009, JCAP, 9, 28

Gott, J. R. I., Jurić, M., Schlegel, D., Hoyle, F., Vogeley, M., Tegmark, M., Bahcall, N., & Brinkmann, J. 2005, ApJ, 624, 463

Guo, Q., et al. 2011, MNRAS, 413, 101

Henriques, B. M. B., White, S. D. M., Lemson, G., Thomas, P. A., Guo, Q., Marleau, G.-D., & Overzier, R. A. 2012, MNRAS, 421, 2904

Hill, D. T., Driver, S. P., Cameron, E., Cross, N., Liske, J., & Robotham, A. 2010, MNRAS, 404, 1215

Huang, J.-S., Cowie, L. L., Gardner, J. P., Hu, E. M., Songaila, A., & Wainscoat, R. J. 1997, ApJ, 476, 12

Huang, J.-S., Glazebrook, K., Cowie, L. L., & Tinney, C. 2003, ApJ, 584, 203

Iguchi, H., Nakamura, T., & Nakao, K. 2002, Progress of Theoretical Physics, 108, 809

Inoue, K. T., & Silk, J. 2006, ApJ, 648, 23

Jarrett, T. H., Chester, T., Cutri, R., Schneider, S., Skrutskie, M., & Huchra, J. P. 2000, AJ, 119, 2498

Johnston, R. 2011, A&A Rev., 19, 41

Jones, D. H., Peterson, B. A., Colless, M., & Saunders, W. 2006, MNRAS, 369, 25

Keenan, R. C., Barger, A. J., Cowie, L. L., & Wang, W. 2010b, ApJ, 723, 40

Keenan, R. C., Barger, A. J., Cowie, L. L., Wang, W.-H., Wold, I., & Trouille, L. 2012, ApJ, 754, 131

Keenan, R. C., Trouille, L., Barger, A. J., Cowie, L. L., & Wang, W. H. 2010a, ApJS, 186, 94

Kirby, E. M., Jerjen, H., Ryder, S. D., & Driver, S. P. 2008, AJ, 136, 1866

Kochanek, C. S., et al. 2001, ApJ, 560, 566

Lavaux, G., & Hudson, M. J. 2011, MNRAS, 416, 2840

Lawrence, A., et al. 2007, MNRAS, 379, 1599

Liske, J., Lemon, D. J., Driver, S. P., Cross, N. J. G., & Couch, W. J. 2003, MNRAS, 344, 307

Lynden-Bell, D. 1971, MNRAS, 155, 95

Maller, A. H., McIntosh, D. H., Katz, N., & Weinberg, M. D. 2005, ApJ, 619, 147

Mannucci, F., Basile, F., Poggianti, B. M., Cimatti, A., Daddi, E., Pozzetti, L., & Vanzi, L. 2001, MNRAS, 326, 745

Marinoni, C., et al. 2005, A&A, 442, 801

Marra, V., Amendola, L., Sawicki, I., & Valkenburg, W. 2013, ArXiv e-prints

Marra, V., & Notari, A. 2011, Classical and Quantum Gravity, 28, 164004

Marra, V., & Pääkkönen, M. 2010, JCAP, 12, 21

Marra, V., Pääkkönen, M., & Valkenburg, W. 2012, ArXiv e-prints

Mishra, P., Célérier, M.-N., & Singh, T. P. 2012, Phys. Rev. D, 86, 083520

—. 2013, ArXiv e-prints

Moffat, J. W., & Tatarski, D. C. 1992, Phys. Rev. D, 45, 3512

—. 1995, ApJ, 453, 17

Moss, A., Zibin, J. P., & Scott, D. 2011, Phys. Rev. D, 83, 103515

Nishikawa, R., Yoo, C.-M., & Nakao, K.-i. 2012, Phys. Rev. D, 85, 103511

Page, M. J., & Carrera, F. J. 2000, MNRAS, 311, 433

Park, C., Choi, Y.-Y., Kim, J., Gott, III, J. R., Kim, S. S., & Kim, K.-S. 2012, ApJ, 759, L7

Planck Collaboration et al. 2013, ArXiv e-prints

Riess, A. G., et al. 2011, ApJ, 730, 119

Sandage, A., Tammann, G. A., & Yahil, A. 1979, ApJ, 232, 352

Schechter, P. 1976, ApJ, 203, 297

Schmidt, M. 1968, ApJ, 151, 393

Sheth, R. K., & Diaferio, A. 2011, MNRAS, 417, 2938

Smith, A. J., Loveday, J., & Cross, N. J. G. 2009, MNRAS, 397, 868

Springel, V., et al. 2005, Nature, 435, 629

Tomita, K. 2000, ApJ, 529, 38

—. 2001a, MNRAS, 326, 287

—. 2001b, Progress of Theoretical Physics, 106, 929

Valkenburg, W. 2012, JCAP, 1, 47

Valkenburg, W., Kunz, M., & Marra, V. 2013, ArXiv e-prints

Valkenburg, W., Marra, V., & Clarkson, C. 2012, ArXiv e-prints

Wang, L., et al. 2012, ArXiv e-prints

Willmer, C. N. A. 1997, AJ, 114, 898

Yoo, C., Kai, T., & Nakao, K. 2008, Progress of Theoretical Physics, 120, 937

York, D. G., et al. 2000, AJ, 120, 1579

Zhang, P., & Stebbins, A. 2011, Physical Review Letters, 107, 041301

Zibin, J. P., Moss, A., & Scott, D. 2008, Physical Review Letters, 101, 251303

Zumalacárregui, M., García-Bellido, J., & Ruiz-Lapuente, P. 2012, JCAP, 10, 9